OCEAN WAVES AND TURBULENCE AS OBSERVED WITH AN ADAPTIVE COHERENT MULTIFREQUENCY RADAR

Dag T Gjessing and Jens Hjelmstad
Royal Norwegian Council for Scientific and Industrial Research,
Environmental Surveillance Technology Programme
P.O. Box 25, N-2007 Kjeller, Norway

ABSTRACT

An adaptive coherent multifrequency radar system has been developed for several applications. By means of this, the velocity distribution (Doppler spectrum) and spectral intensity of 15 different irregularity scales (waves and turbulence) can be measured simultaneously. Changing the azimuth angle of the antennas at regular intervals, the directivity of the wave/turbulence pattern on the sea surface can also be studied.

Using this radar system, series of measurements for different air/sea conditions have been carried out from a coast-based platform in Southern Norway. Experiments in the Atlantic were also performed with the same equipment making use of the NASA Electra aircraft.

There are many air/sea phenomena which play a role in relation to backscattering of radio waves in the microwave region: gravity waves "modulate" the capillary wave structure, overturning wave crests produce focussing effects and also periodic regions of strong turbulence, the boundary layer wind field with strong turbulence amplified by the ocean waves will conceivably leave a patchy and even periodic footprint on the sea surface.

By virtue of the fact that our multifrequency radar allows us to measure the velocity distribution ("coherent and incoherent component") associated with 15 different ocean irregularity scales simultaneously in a directional manner, it is possible to study the different air/sea mechanisms in some degree of detail.

1 INTRODUCTION

Radio methods have a substantial potential in the study of the irregularity structure of the sea surface for several reasons:

- They provide a rather unique possibility to measure the directional wave spectra with good directional resolution
- By means of a multifrequency radio method wavelength and wave velocity can be measured independently
- It is also possible to distinguish between coherent wave motion and incoherent motion (turbulence)

We shall present a detailed theoretical and experimental study of the sea surface. We shall in particular demonstrate that a microwave illuminator can be tailored so as to optimize the coupling between electromagnetic waves and ocean waves.

There are three different problem areas:

A. One must obtain an understanding in regard to the coupling mechanisms between the electromagnetic waves on the one hand, and the sea surface on the other.

B. Having established information about the sea surface as a scattering surface for radio waves (the delay function $f(\vec{r},t)$ or the spectrum $E(\vec{K},\omega)$), it remains to establish the relationship between this "description domain of the radio scientist" and that of the ocean scientist, who want information about most significant wave-height, wave-height spectra etc.

To convert from scattering cross-section to wave-height one needs information about how gravity waves and other large scale phenomena affect the small scale phenomena (capillary waves) which are comparable with the wavelength of the radio field and which are responsible for the scattering.

C. One needs an understanding of the fundamental hydrodynamic mechanisms.

In the current contribution we shall confine ourselves to problem area A. the interaction between electromagnetic waves and an irregular ocean surface. (See also Gjessing, Hjelmstad, Lund (1984)).

2 SCATTERING FROM A ROUGH SURFACE

2.1 A summary of basic theory

In recent contributions (Gjessing, 1981 a and b), a somewhat detailed discussion was presented of the properties of the electromagnetic field scattered from a rough surface.

The basic scattering equation can be expressed as

$$E_s(\vec{K},t) \sim \int_{-\infty}^{\infty} f(\vec{r},t)\, e^{-j\vec{K}\cdot\vec{r}}\, d^3\vec{r} \qquad (2.1)$$

$$\vec{K} = \vec{k}_j - \vec{k}_s \quad \text{and} \quad |\vec{K}| = \frac{4\pi}{\lambda} \sin\theta/2$$

λ is wavelength and θ scattering angle.

In order to obtain backscatter from a scattering surface, the surface must have a structure, regular or irregular, containing scale sizes $L = \frac{2\pi}{K} = \lambda/2$.

Referring again to equation (2.1), $\vec{r}$ is a position vector, t is time and $f(\vec{r})$ is the delay function characterizing the surface. This complex function tells us how the scattering elements contributing to the "bulk scattering cross-section σ" are distributed spatially.

Resolving $\vec{r}$ and $\vec{K}$ into orthogonal coordinates in the horizontal plane

$$E(\vec{K}) \sim \{\int_{-\infty}^{\infty} f(z)\, e^{-jK_z z}\, dz\}\, \delta(K_x x) \qquad (2.2)$$

where δ denotes a Dirac delta function.

The scattered field $E(K)$ vanishes unless K_x is zero. Hence, $E(\vec{K}) = 0$ unless $\vec{K}$ is normal to the wave crest.

Let us assume that we illuminate the sea surface with a beam whose width is limited so as to cut out a section D of the ocean wave front (see figure 1).

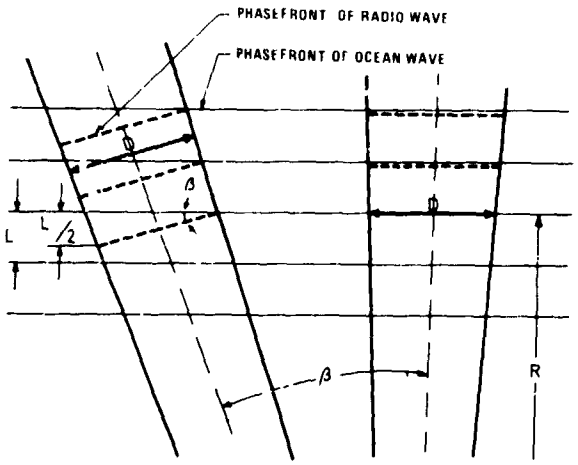

Figure 1 The geometry of the truncation (convolution) process

$$\beta = \tan^{-1}\left(\frac{L}{2D}\right)$$

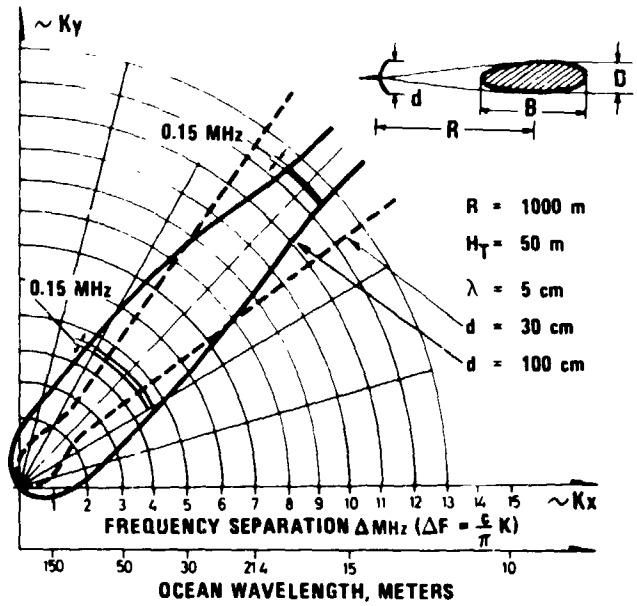

Figure 2 The angular resolution of our radar varies with ocean wavelength. As the ocean wavelength decreases, the resolution approaches that of the antenna beamwidth.

In this case $E(K_x)$ will be of a sine form instead of the Dirac delta function when approximating the antenna beam function to a rectangular distribution.

Thus, if D be the width of the truncation influencing $f(x)$, and $K = \frac{2\pi}{L}$ be the wavenumber of the one-dimensional delay function $f(z)$, (L is the ocean wavelength) then the angular width (angle between nulls) 2α of the $E(K_x)$ function is

$$2\alpha = \frac{L}{D} \tag{2.3}$$

This is a relationship well known from antenna theory. The beamwidth 2α (azimuth resolution) is determined by the antenna aperture D expressed in wavelengths L. (See figure 1).

This is illustrated in figure 2 and verified experimentally in figure 13.

The radar antenna is illuminating a range interval B measured along the direction of wave propagation. This leads to a truncation of the delay function $f(\vec{r})$. Then $\delta F_{\frac{1}{2}} = 0.16\,\frac{C}{B}$ for an exponential function (Gjessing 1981b).

We shall now suggest a simple mathematical model based on basic and rather intuitive physical arguments to provide a simple way of assessing the experimental findings. We assume that long ocean waves (wavenumber approaching cut-off K_o) are unidirectional. The higher the wavenumber, the larger is the angular spread. For waves in the wavenumber region above K_s, the irregularity structure is isotropic. We therefore write the complex irregularity spectrum simply as

$$E(\vec{K}) = E(|\vec{K}|, \theta)$$

$$\sim K^{-n}(\cos\theta)^s$$

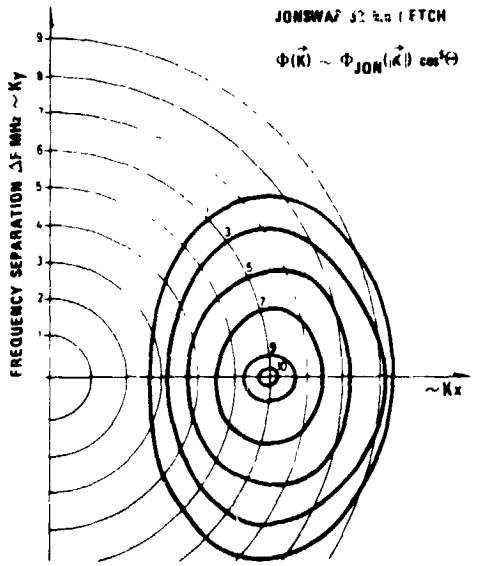

Figure 3 Complex wave spectrum calculated from the simple model presented

$K_o = 0$, $K_s = \frac{2\pi}{5}\ m^{-1}$

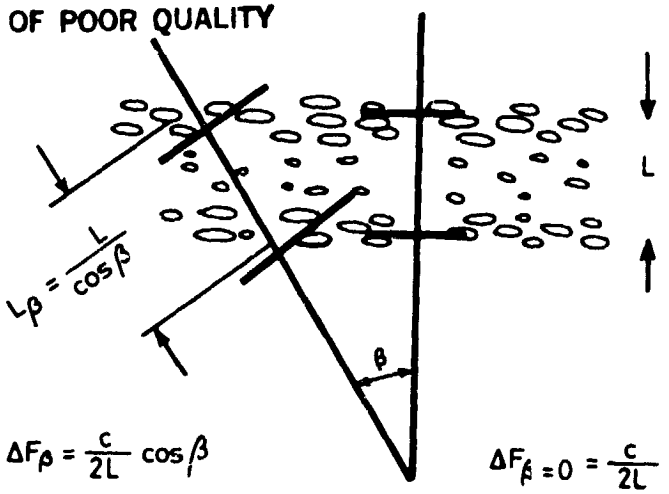

Figure 4 Scattering from turbulent irregularities caused by the "footprint" of a local wind field interacting with the wave structure of the sea

where s, the planeness parameter, is expressed as

$$s = \frac{K_s - K}{K - K_o}$$

where K_o is the wavenumber corresponding to the short wavenumber cut-off, and K_s is the wavenumber at which the ocean surface structure becomes "random" and isotropic with no prevailing wave direction.

A local wind field may through shear mechanisms break up the coherency of the ocean wave ridge. The effect of this is to widen the angular distribution of the back-scattered radar wave considerably, as illustrated in figure 4.

Here we have obtained that the wave crests and troughs are broken up by turbulence and wave backing phenomena such that there is no "phase matching" between radio wave and ocean wave over the illuminated area contrary to the coherent case depicted in figure 1.

Thus, when turning the antennas on azimuth angle β, the radio wave sees a dominating ocean irregularity scale which is increased from L when β=0 to

$$L_\beta = \frac{L}{\cos\beta}$$

This is illustrated in figure 4. Note that for certain values of K (and the corresponding ΔF) the back-scattered radio signal will increase with increasing azimuth angle symmetrically on either side of the β=0 direction. For experimental verification, the reader is referred to figures 11 and 13.

It is well known from turbulence theory that the nearness of a rough boundary such as the sea surface results in a low wavenumber suppression of the turbulence field

and also to anisotropy (see e.g. H Panovsky 1960). (Modulation of the sea surface by the wind turbulence, anisotropic irregularity structure on the sea surface with an axis of symmetry determined by the direction of the local mean wind (Gjessing 1962).)

2.2 The multifrequency radar principle, frequency difference matching

Up to this point we have been dealing with electromagnetic waves having wavelengths which are comparable with the irregularity scale of the scattering surface.

We shall now investigate what information we can derive by matching some beat patterns (difference frequency) to the irregularity scales of the sea surface. Figure 5 illustrates the physics of the problem.

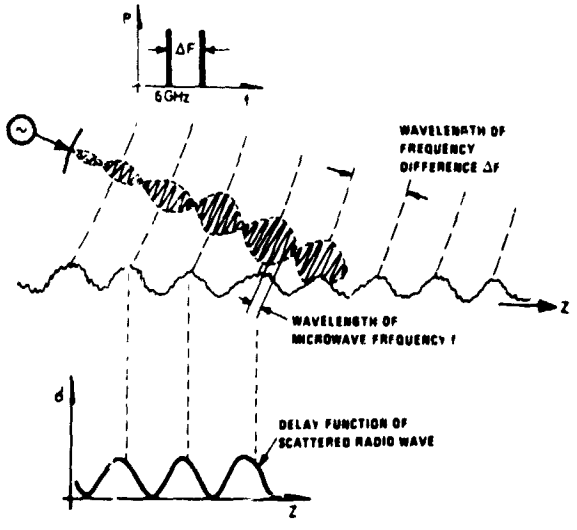

Figure 5 The interaction of electromagnetic waves with the sea surface

For this ΔK matching scheme to work (see e.g. Plant 1977), the scattering surface obviously must have irregularities which contribute to the delay function $f(z)$ for scales corresponding to the difference wavenumber ΔK. If the gravity wave structure shows up in the delay function $f(z)$, i.e. if the spectrum of $f(z)$ has Fourier components matching the wavenumber ΔK, we would experience a radar return at the beat frequency $\Delta\omega = c\Delta K$.

There are many ostensible explanations for this "modulation" of the small scale structure (to which the wavenumber $\vec{K}$ is matched) by the long wave phenomena (to which ΔK is matched). (See e.g. Plant 1977, Plant and Schuler 1980).

It is well known that the scattering cross-section of a surface increases with incidence angle. From a sinusoidal gravity wave we shall get maximum low angle return at the point of maximum slope. The turbulent intensity is governed by damping factors such as shear forces (Lumley 1969). Orbital motion within the wave structure changes the velocity shear periodically in phase with the gravity wave. Shadowing effects may enhance the patchiness of the radar illumination. Breaking waves and white capping resulting from the local wind field etc complicates the issue still further.

Having presented intuitive arguments based on physical interpretations, now let us describe the principle of the multifrequency radar mathematically.

We start with the simple and general expression given earlier

$$V(\tfrac{\omega}{c}) \sim E(\vec{K}) \sim \int_V f(\vec{z})\, e^{-j\vec{K}\cdot\vec{z}}\, d^3\vec{z} \qquad (2.4)$$

and we compute the covariance $E(\vec{K})\, E^*(\vec{K}+\Delta\vec{K})$ obtaining

$$\overline{E^*(\vec{K})\, E(\vec{K}+\Delta\vec{K})} \sim e^{-j\Delta\vec{K}\cdot\vec{z}} \cdot \int R(\vec{r})\, e^{-j\vec{K}\vec{r}} \cdot e^{-j\Delta\vec{K}\vec{r}}\, d^3\vec{r} \qquad (2.5)$$

$R(\vec{r})$ is the complex autocorrelation of the delay function $f(z)$. The phase factor

of the autocorrelation function (the term $e^{-j\Delta\vec{K}\cdot\vec{z}}$) is rapidly oscillating with $\Delta\vec{K}$ since the space coordinate $\vec{z}$ is large.

The factor $e^{-j\vec{K}\vec{r}}$ represents the modulation of the spatial autocorrelation function by the radar carrier. But as the radar wavelength (5 cm) is orders of magnitude smaller than the scales of interest on the sea surface, this factor will not affect the measured sea-surface signature because the individual scatterers move independently such that the effect of the rapidly rotating phase factor will be averaged out.

This can also be argued for mathematically by noting that the integral is of the form of a Fourier integral which is symmetrical with respect to $\vec{K}$ and $\Delta\vec{K}$. Taking $\vec{K}$ and $\vec{r}$ as the Fourier pair of variables, and making use of the fact that the Fourier transform of a product is equal to the convolution of the Fourier transform of each factor, the integral converges to

$$\int_V R(\vec{r})\, e^{-j\Delta\vec{K}\vec{r}}\, e^{-j\vec{K}\vec{r}}\, d^3\vec{r} = \delta(\vec{K}) \ast \Phi(\vec{K}-\Delta\vec{K}) = \Phi(\Delta\vec{K}) \qquad (2.6)$$

where $\ast$ denotes convolution and δ is Dirac's delta function. $\Phi(\Delta\vec{K})$ is the wavenumber spectrum which again is the Fourier transform of the spatial autocorrelation function $R(\vec{r})$.

As $\vec{K} >> \Delta\vec{K}$, the term $\Phi(\vec{K})$ will vanish because $\vec{K}$ assumptionally is greater than the scattering medium cut-off wavenumber. As an example, note that if $\frac{K}{\Delta K} = 1000$, $\Phi(K)/\Phi(\Delta K) = 10^6$ for a rectangular distribution of scattering elements.

Normalizing this expression, we get the following familiar expression for a given fixed monostatic transmitter/receiver position

$$\frac{E^*(\frac{\omega}{c})\, E(\frac{\omega+\Delta\omega}{c})}{\overline{|E(\frac{\omega}{c})|^2}} = \frac{e^{-j\frac{\Delta\omega}{c}z} \int R(r)\, e^{-j\frac{\Delta\omega}{c}\cdot r}\, d^3r}{A} \qquad (2.7)$$

where A is a normalizing factor of the form $\int R(r)\, dr$.

Equation (2.7) states that the envelope of the complex correlation in the frequency domain of waves scattered back from a surface is given by the autocorrelation function $R(r)$ characterizing the surface.

2.3 The motion pattern of the sea surface

In the section above, we have shown that frequency components with mutual frequency spacing F couple to irregularity scale sizes $\Delta L = \frac{c}{2\Delta F}$.

We have already observed that the irregularity structure (the delay function) of the sea surface is determined by several mechanisms. Gravity waves are well behaved, and propagate at a velocity

$$v = \sqrt{\frac{g}{K}} = \sqrt{\frac{gL}{2\pi}} \qquad (2.8)$$

where L is the wavelength.

Since the Doppler shift produced by a scatterer at velocity $\vec{v}$ is given by $f = \frac{1}{2\pi}\vec{K}\cdot\vec{v}$

$$f = \frac{2\Delta F}{c}\sqrt{\frac{gL}{2\pi}} \qquad (2.9)$$

giving

$$f = \sqrt{\frac{g\Delta F}{\pi c}} \tag{2.10}$$

We select a given ΔF_1 (which is the same as selecting a given irregularity scale L_1), and we measure how the frequency covariance function

$$R(\Delta F_1, t) = V(F,t)\ V^*((F+\Delta F_1),t)$$

is varying with time t. We then compute the power spectrum of the frequency covariance function $R(\Delta F_1 t)$.

If then the ordered gravity waves dominate over the incoherent velocity components which ride on the gravity waves, we would expect the Doppler spectrum to have a maximum at the frequency corresponding to the dispersion relation of gravity waves (eq (2.10) above), and we would expect a Doppler broadening determined by the velocity spread δV.

3 EXPERIMENTAL RESULTS

The adaptive multifrequency radar system developed by the authors' organization has been used for several applications: ship and aircraft identification, measurement of sea surface from a ground-based station and from an aircraft. A brief highlighting of results related to the sea surface will now be given.

3.1 Directional ocean wave spectra observed from the NASA Electra aircraft

Illuminating the sea surface by a fixed 14° beamwidth side-looking antenna pointing 10° downwards relative to the horizontal plane, the ocean wave spectra were determined for various azimuth directions and for 15 different ocean wavelengths in the interval from some 16 m (couples to ΔF = 8 MHz) to 300 m (corresponding to ΔF = 1/2 MHz). For each frequency separation ΔF the frequency covariance function $V(F,t)\ V^*(F+\Delta F,t)$ was computed.

The NASA Electra operated north-east of Wallops Flight Facility (38.49.2 N - 74.24 W) at an altitude of 12 000 ft, January 20, 1983, time 2203Z.

Banking the aircraft 10° so that the antennas were pointing at a depression angle of 20°, the aircraft completed a 360° circle. In this way the antenna was illuminating essentially the same area on the sea surface at all azimuth directions. The longitudinal dimension of the footprint is approximately 5600 m, whereas the transverse dimension is approximately 2000 m.

Flying in a closed circle, the frequency covariance function $V(F)\ V^*(F+\Delta F)$ was computed for 15 different values of ΔF for all azimuth angles. The results are shown in figure 6. Note that the Bragg angle is clearly visible for the longer wavelengths (215 - 88 m).

In terms of aircraft altitude H, depression angle α and antenna beamwidth $\Delta\beta$ we get the following expression for the Bragg angle

$$\beta = \frac{L}{2H}\ \frac{\sin\alpha}{\sin(\frac{\Delta\beta}{2})}$$

This is presented in figure 7. Note the good agreement between theory and experimental results.

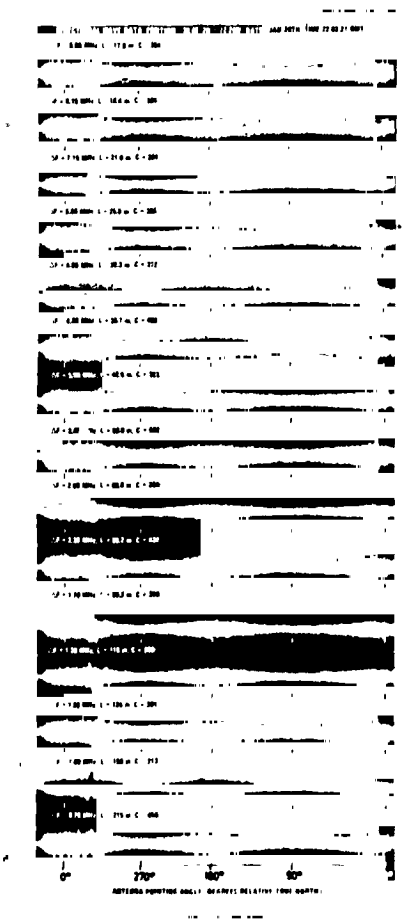

Figure 6

The aircraft flew in a closed circle pointing the antennas 30° down from 12 000 ft. The covariance function $V(F)V^{*}(F+\Delta F)$ is shown for 15 different values of ΔF.

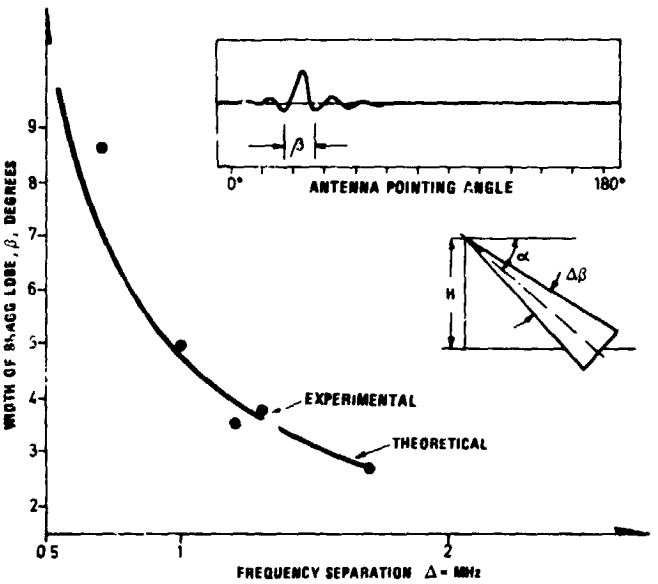

Figure 7 The measurement of Bragg angle is compared with theory. Note that the aircraft altitude is 12 000 ft, depression angle 30° and beamwidth 14°.

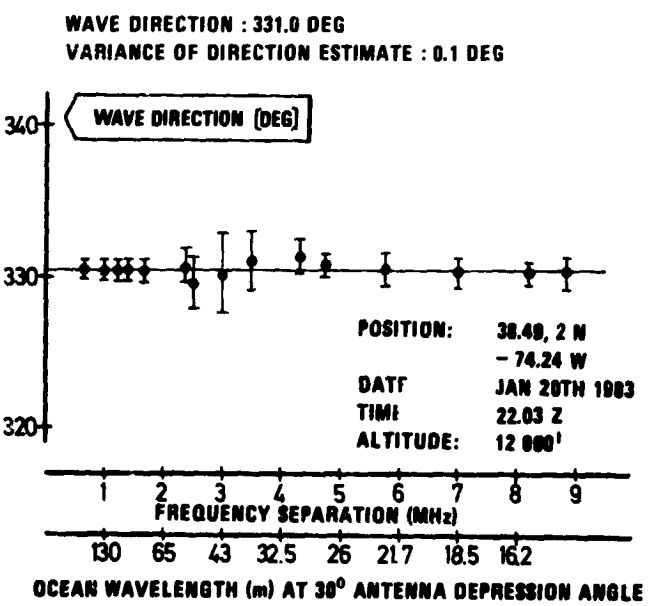

Figure 8 Wave direction plotted as a function of wavelength

Noting the two azimuth angles corresponding to destructive interference on either side of the wave direction, this can be determined with great precision as shown in figure 8.

Finally, for an azimuth direction corresponding to that of the propagation direction of the ocean waves, the distribution with wavelength of the scattering cross-section is computed. This is shown in figure 9. Note that two wavelengths dominate, 130 m and 18 m.

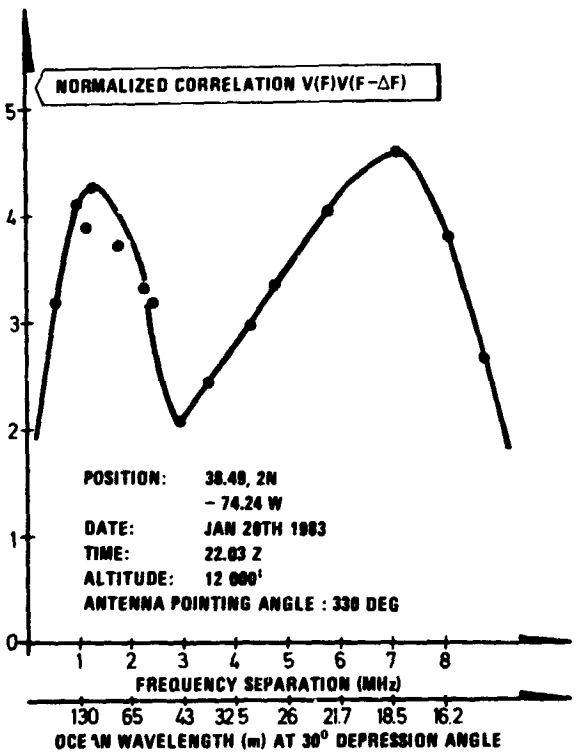

Figure 9 There are two dominating wavelengths, 130 m and 18 m.

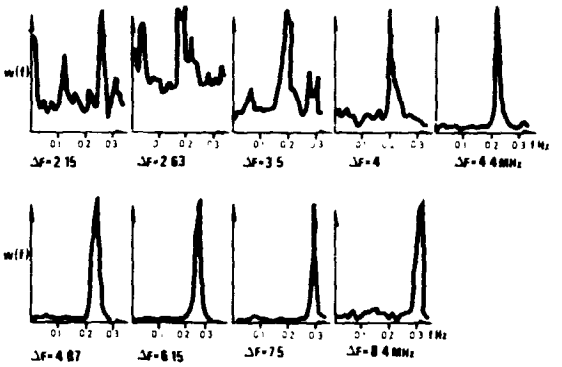

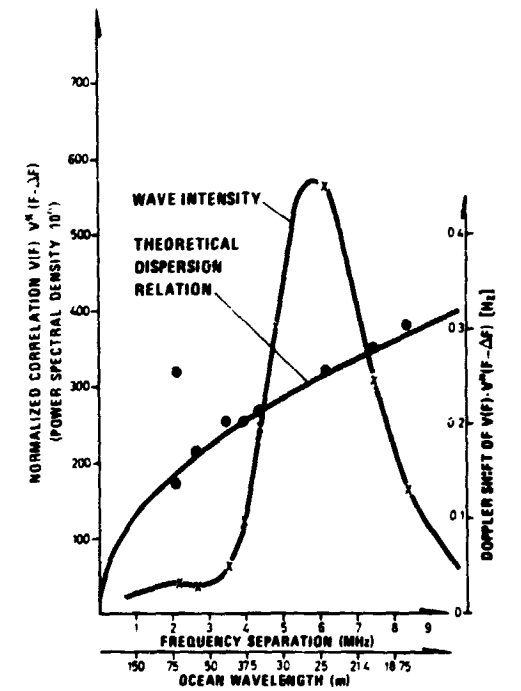

Figure 10 Spectra of wavelength and wave velocity. Note that wavelengths shorter than that corresponding to the spectral peak move at constant velocity. This is not the case for longer scales. The results are from Langesund 12 March 81 at 1030 local time, the azimuth direction being 137°.

3.2 Directional spectra obtained from ground-based station on a cliff

The complex field strength was recorded over a period of some 12 minutes before the azimuth angle was changed, thus obtaining a plot of power spectral density and Doppler spectrum as a function of frequency separation (ocean wavelength). A typical result is shown in figure 10.

First, consider the results obtained on March 12, 1981 (1010 - 1235 local time). The weather and sea state can be characterized as follows:

- Wind direction 90^{o} (East)
- Wind speed approximately 8 m/s
- Wave height 1.4 m peak to peak
- Waverider gives maximum wave height for f = 0.225 Hz
- Wind decreasing at noon, turning northerly. Wave height reduces to 1 m peak to peak, choppy sea

Figure 12 shows the wave intensity for a particular azimuth direction and also the Doppler spectra associated with various scale sizes. Note the very well defined spectral peak in the intensity versus wavelength distribution. Note also that the Doppler frequency is in very good agreement with the theoretical dispersion relation. There seems to be a slight, but consistent, displacement to higher Doppler frequency. This is a result of an inward current.

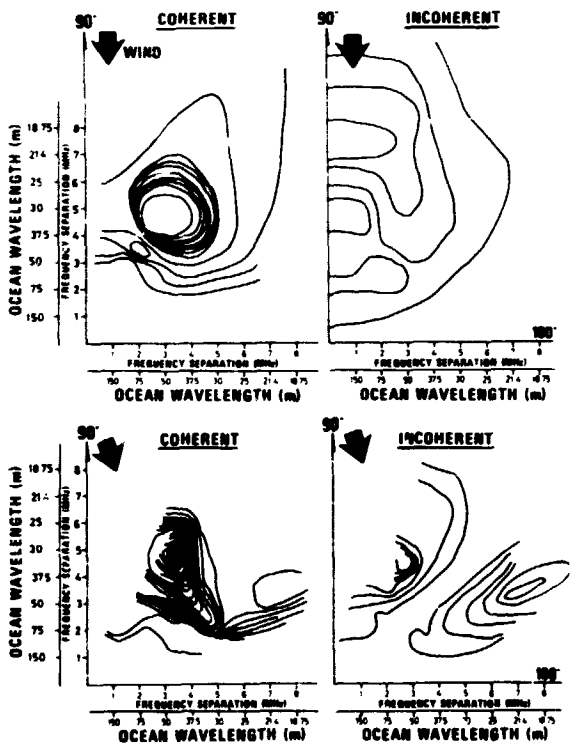

Figure 11 Isolines of spectral intensity $\Phi(\Delta\vec{K})$ in the K_x-K_y plane. Note the effect of changes in wind direction on the coherent irregularity spectrum. Note that the upper set of maps was obtained on 12 March 1981, 1010 to 1135 local time, whereas the lower set refers to the situation during the time interval 1135 to 1235.

Finally, in figure 11, we present the two-dimensional irregularity spectrum summing up the description of the sea-surface structure. Here we have plotted the isolines of spectral intensity, or more specifically the quantity $V(F)\ V^{*}(F+\Delta F)/V(F)^{2}$, in the K_x-K_y plane. This presentation should be compared with those of figures 2, 3 and 4. Note also that the isolines of spectral intensity $\Phi(\Delta\vec{K})$ are obtained directly from a set of one-dimensional spectra such as those shown in figure 10.

As will be seen, we distinguish between coherent and incoherent components. With "coherent component" we refer to the dominant Doppler spectral line caused by the "coherent" gravity wave $(f = \sqrt{\frac{g\Delta F}{\pi c}})$.

The incoherent component is the "residue intensity" of the Doppler spectrum (the contribution from the skirts) obtained when the coherent contribution wave is subtracted. It can be visualized as all the random turbulent velocity contributions outside the short velocity interval dominated by the gravity wave. Note, however, that although the velocity of the scatterers vary widely as seen e.g. from figure 10, the difference frequency ΔF selects a narrower range of irregularity scales centered round the scale size L given by

$$L = \frac{c}{2\Delta F}$$

If these weak incoherent irregularities were entirely due to the local wind field, one would expect the local wind direction to provide an axis of symmetry. Unfortunately, the antenna systems were not flexible enough to be turned beyond the east direction ($\theta = 90^{o}$). It is therefore difficult to establish such a symmetry. The coherent contribution, however, has a pronounced axis of symmetry determined by the direction of the most energetic ocean wave. We see that the angular distribution is far from $\cos^2\theta$ distributed, long waves are more plane than the shorter ones, as suggested in figure 3.

The lower set of directional spectra in figure 11 gives the situation one hour later when the wind has turned from east towards north. We see that the most energetic waves (the "eye" of the isoplot chart) have not changed direction, whereas the shorter scales and weaker disturbances are reoriented slightly. The distribution of the incoherent (turbulent) irregularities is drastically altered.

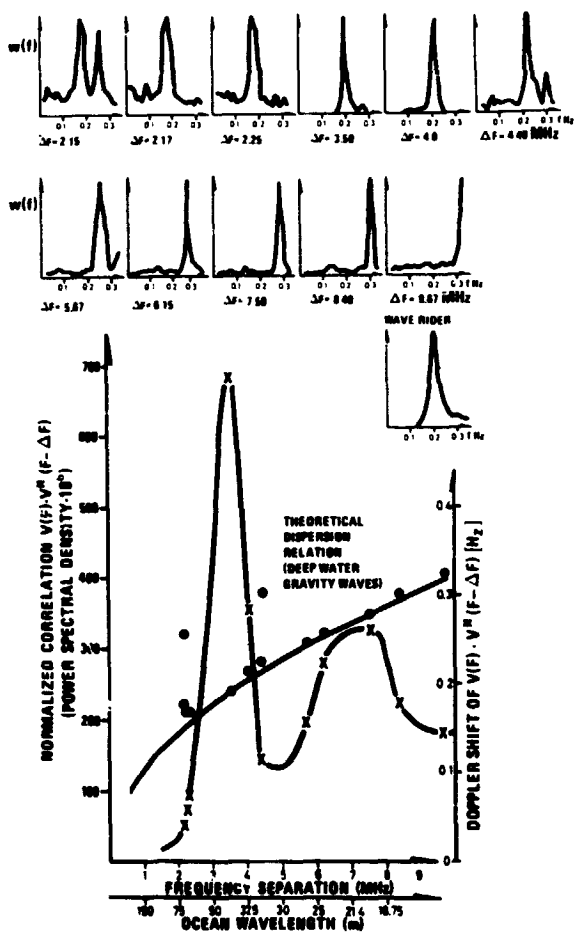

Figure 12 Spatial and temporal wave spectra for an azimuth direction of 140°. Location is Langesundsfjorden, time is 18 March 81, 1525 local time

On 18 March 1981 there is no wind before noon. At 1330 the wind speed is 10 m/s from south, bringing the water height up to 2.5 m. The complex K plot shows a unidirectional spectrum.

Two hours later, when the wave height has increased to 2.5 m peak to peak, and wind has turned easterly, the irregularity structure is very much altered. This most striking feature has (as indicated in figure 12 and also summarized in figure 13) the very pronounced appearance of a second peak at a wavelength of 25 m whereas the dominating spectral peak is still 50 m. Note that this two-peak spatial spectrum for a particular azimuth direction is not very pronounced in the wave-rider spectrum. This, presumably is a result of the omnidirectional response pattern of the wave-rider. Note also that figure 12 shows a very pronounced two-peak structure in the Doppler spectrum for an ocean wavelength of some 70 m. Finally, figure 13 sums up the results of the afternoon run in the form of $\Phi(\Delta\vec{K})$ isolines for the coherent as well as for the incoherent components. Note that the wavelength corresponding to peak spectral intensity varies with azimuth angle.

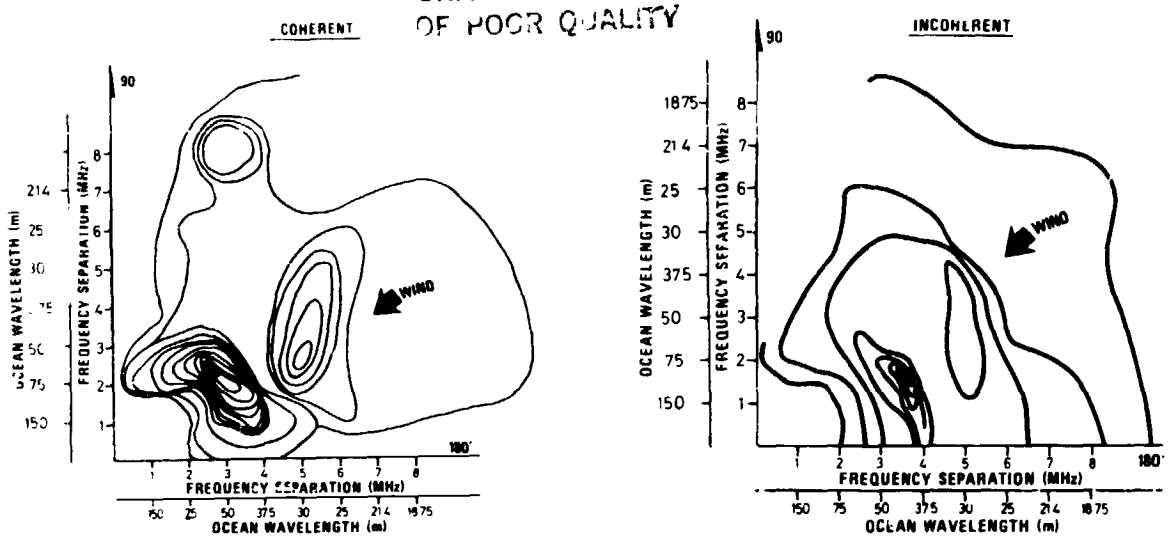

Figure 13 The two-dimensional ocean irregularity spectrum (isolines of $\Phi(\Delta\vec{K})$) when the wave height has increased to 2.5 m peak to peak and the wind has turned towards east

Acknowledgements

The authors would like to acknowledge the very valuable services rendered by Dr Dagfin Brodtkorb and Jan Wøien of A/S Informasjonskontroll who laboriously and conscientiously did all the data recording and computer data reduction. They also developed most of the computer software and played a very active role in the planning of the data analysis.

The authors would also like to acknowledge the contribution by Dr Anton Kjelaas who developed much of the basic software and took part in the preliminary campaigns.

The multifrequency radar is based on a 960 channel radio relay link generously provided by Mr Bjarne Standahl of Elektrisk Bureau, Division NERA, and the waverider and wind measuring equipment was generously provided by Dr Torkild Carstens of the Norwegian Hydrodynamic Laboratories.

The sea surface measurements performed from the NASA Electra aircraft were made possible by the kind invitation of Dr David Atlas of NASA for which the authors are much indebted.

REFERENCES

Alpers, W.R., and K. Hasselmann, 1978: The two-frequency microwave technique for measuring ocean wave spectra from an airplane or satellite. Boundary Layer Meteorol, 13, 215-230.

Barrick, D.E., 1972: First order theory and analysis of MF/HF/VHF scatter from the sea. IEEE Trans AP-20.

Bass, F.G. and I.M. Fuks, 1979: Wave scattering from statistically rough surfaces. Pergamon Press.

Bretherton, E.P., 1969: Waves and turbulence in stratified fluids. Radio Sci, 4, 1279-1287.

Clifford, S.F. and D.E. Barrick, 1978: Remote sensing of sea state by analysis of backscattered microwave phase fluctuations. IEEE Trans AP-26, 699-705.

Gjessing, Dag T., 1962: On the scattering of electromagnetic waves by non-isotropic inhomogeneities in the atmosphere. J Geophys Res, 67, 3.

Gjessing, Dag T., 1964: Determination of isotropy properties of the tropospheric permittivity and wind velocity fields by radio-propagation methods. J Geophys Res 69, 4.

Gjessing, Dag T. and F. Irgens. 1964a: On the scattering of electromagnetic waves by a moving tropospheric layer having sinusoidal boundaries. IEEE Trans AP-12.1.

Gjessing, Dag T. and F. Irgens, 1964b: Scattering of radio waves by moving atmospheric rippled layers: A simple model experiment. IEEE Trans AP-12.6.

Gjessing, Dag T, 1981a: Adaptive techniques for radar detection and identification of objects in an ocean environment. IEEE J Ocean Engineer, OE-6.1

Gjessing, Dag T., 1981b: Adaptive radar in remote sensing. Ann Arbor Science Publisher Inc.

Gjessing, Dag T., J. Hjelmstad and T. Lund, 1982: A multifrequency adaptive radar for detection and identification of objects. Results of preliminary experiments on aircraft against a sea-clutter background. IEEE Trans AP-30, 3, 351-365.

Gjessing, Dag T, J. Hjelmstad and T. Lund, 1984: Directional ocean wave spectra as observed with multifrequency continuous wave radar. Review paper in International Journal of Remote Sensing, January 1984.

Hasselmann, K. et al., 1973: Measurements of wind-wave growth and swell decay during the Joint North Sea Wave Project (JONSWAP). Ergänzungsheft zur Deutschen Hydrographischen Zeitshrift. Reihe A/80, 12.

Jones, L. and D.E. Wiessman, 1981: The two frequency microwave scatterometer measurements of ocean wave spectra from an aircraft. Oceanography from Space. Proc. COSPAR/SCOR/IUCRM Symposium, ed. J.F.R. Gower. Plenum Press, N.Y.

Lumley, J.L., 1967: Theoretical aspects of research on turbulence in stratified flows. Atmospheric turbulence and radio wave propagation, ed. A.M. Yaglom and V.I. Tatarsky. Publishing House NAUKA, Moscow, pp 105-112.

Panowsky, H.A. and R.A. McCormick, 1960: The spectrum of vertical velocity near the surface. Quart J Ray Met Soc.

Phillips, O.M., 1969: The dynamics of the upper ocean. Cambridge Univ.Press, p 159-.

Plant, W.J., 1977: Studies of backscattered sea return with a CW dual-frequency X-band radar. IEEE Trans AP-25, 1.

Plant, W.J. and D.L. Schuler, 1980: Remote sensing of the sea surface using one and two frequency microwave. Radio Sci, 15, 3, 605-615.

Schuler, D.L., 1978: Remote sensing of directional gravity wave spectra and surface currents using a microwave dual-frequency radar. Radio Sci, 13, 2.

Tatarsky, V.E., 1961: Wave propagation in a turbulent medium, translated by R.A. Silverman. McGraw-Hill, New York.

Tomiyasu, K., 1971: Short pulse wide-band scatterometer ocean surface signature. IEEE Trans GE-9, 175-177.

Valenzuela, G.R., 1978: Scattering of electromagnetic waves from the ocean. Surveillance of environmental pollution and resources by electromagnetic waves. Proc. NATO Advanced Study Institute, Spåtind, Norway 9-19 April 1978. ed. T.Lund.

Waterman, A.T., D.T. Gjessing and C.L. Liston, 1961. Statistical analysis of transmission data from a simultaneous frequency- and angle scan experiment. Contribution to the URSI Spring Meeting, Washington DC., 1961.

Weissman, D.E. and J.W. Johnson, 1977: Dual frequency correlation radar measurements of the height statistics of ocean waves. IEEE J Ocean Engineer, OE-2. 74-83.

Weissman, D.E., J.W. Johnson and J.T. Ramsey, 1982: The delta-K ocean wave spectrometer: Aircraft measurements and theoretical system analysis. Proc. IGARSS -82.

Woods, J.D., 1969a: On Richardson's number as a criterion for laminar-burbulent-laminar transition in the ocean and atmosphere. Radio Sci, 4, 12, 1289-1298.

Wright, J.W., 1968: A new model for sea clutter. IEEE Trans AP-16. 217-223.

Wright, J.W., W.J. Plant, W.C. Keller and L. Jones, 1980: Ocean wave-radar modulation transfer functions from the West Coast Experiment. J Geophys Res. 85, C9, 4657-4966.